E-Journal of Advanced Maintenance Vol.5-1 (2013) 51-61
Japan Society of Maintenology

Novel Mode Decomposition Algorithms for Lamb Wave Signal Analysis in Online Monitoring of Structures

Oleksii KARPENKO[1,*], Gerges DIB[1], Mahmoodul HAQ[2], Lalita Udpa[1] and Satish UDPA[1]

[1]*Non-Destructive Evaluation Laboratory, Michigan State University, Electrical and Computer Engineering Department, East Lansing, 48822, MI, USA*
[2]*Composite Vehicle Research Center, Michigan State University, East Lansing, 48910, MI, USA*

ABSTRACT

Guided wave (GW) inspection systems offer the capability for online health monitoring of structures and hence the potential for transitioning from schedule-based maintenance to conditioned-based maintenance of nuclear plants. However, a major problem in guided wave NDE is the presence of multiple propagation modes at any actuation frequency that travel with different velocities and interfere with each other which makes interpretation of GW signals complicated. Decomposition of the measured signal into its constituent components is a critical requirement for accurate analysis in terms of detection, location and characterization of structural defects. This paper addresses the above problem using a new two-stage Mode Decomposition (MD) algorithm. The first stage employs fast high-resolution Time-Frequency Representation (TFR) of the signal based on Reassigned Spectrogram with Chirp Transform kernel (RSCT), which is used for preprocessing. The second stage includes efficiently implemented Matching Pursuit with dispersion-based dictionary. The performance of the algorithm is demonstrated on 2-mm thick aluminum plates with surface-bonded piezoelectric wafer sensors. The results show that the algorithm identifies the modes and separates closely spaced or overlapped S0 and A0 wave packets. Automated analysis of the MD output allows for detection of flaw indications corresponding to different modes using standard diagnostic imaging algorithm.

KEYWORDS

Lamb waves, online monitoring, multimodal signal, mode decomposition, reassigned spectrogram with chirp transform kernel, matching pursuit, dispersion-based dictionary, diagnostic imaging.

ARTICLE INFORMATION

Article history:
Received 28 November 2012
Accepted 14 March 2013

1. Introduction

1.1. Online monitoring using guided waves

Implementation of online monitoring systems is essential for improving reliability and competitiveness of nuclear power plants. Current methods for ensuring safe operation include eddy current inspection of critical components carried out when the plant is shut down. However, real-time NDE of structures and pipes conveying flow between the primary and secondary sides is no less important. In recent years, guided wave (GW) systems have shown their capability for continual health monitoring of such structures, which offers potential for reducing costly schedule-based maintenance [1]. The advantage of guided waves or Lamb waves is their ability to propagate long distances with minimal attenuation, to follow curvature of the sample, and their sensitivity to defects such as cracks, delaminations and corrosive degradation in materials. However, the analysis of GW signals and damage identification still remains a challenge. Complexity of guided wave inspection is largely due to the presence of multiple symmetric and anti-symmetric modes actuated in the structure (Fig.1b-c). Depending on frequency, each of these modes appears in different harmonics and may propagate with different velocities resulting in dispersion of wave packets. For a media with known material properties and geometry, phase and group velocity dispersion curves (Fig.1a) can be calculated by solving Rayleigh-Lamb equation [2].

*Corresponding author, E-mail: karpenko@msu.edu

ISSN-1883-9894/10 © 2013 – JSM and the authors. All rights reserved.

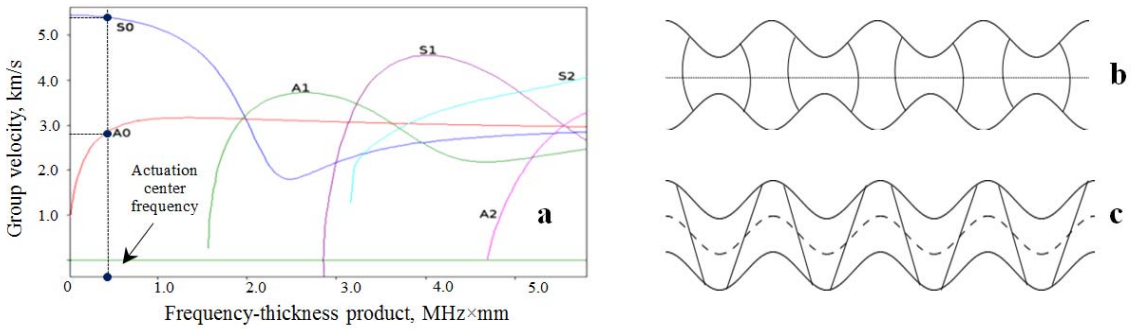

Figure 1. a) Dispersion curves of aluminum plate; b) symmetric modes; c) antisymmetric modes.

Existing devices for Lamb wave actuation and sensing (e.g. piezoelectric transducers, EMATs, etc.) are not strictly mode selective and omnidirectional. Hence, in many cases multiple modes propagate in the structure with different velocities, interfering with each other and with reflections from edge and defect, which makes interpretation of GW signals complicated.

This paper presents a signal processing method for the analysis of guided wave data in terms of detection, location and characterization of structural defects. The proposed method combines high-resolution time-frequency representation (TFR) with matching pursuit (MP) in order to decompose Lamb wave signals into constituent modes using dispersion-based dictionary. When the mode decomposition of the input signal is completed, the algorithm extracts information about the amplitude, Time-of-Flight (ToF) and distance travelled by each wave packet detected. The above features are of great importance, because they allow for accurate damage assessment and diagnostic imaging [3].

2. Time-Frequency Analysis of Lamb Wave Signals

2.1. Conventional time-frequency representations

Time-frequency representation determines the instantaneous frequency and phase of the signal as it changes over time. In GW analysis, TFR is usually followed by processing of spectral images in order to locate their time-frequency centers and identify reflections. One of the simplest examples of a TFR is the Short Time Fourier Transform (STFT). The GW signal to be processed is multiplied by a window function with a short time support. Then the Fourier Transform of the signal within the window is taken as it moves along the time axis. This results in a two-dimensional time-frequency representation

$$S(t,\omega) = \frac{1}{2\pi}\int_{-\infty}^{\infty} s(\tau)h(\tau - t)e^{-j\omega\tau}\,d\tau\,, \tag{1}$$

where $s(t)$ – signal, $h(t)$ – window function, τ – time lag variable, and ω – radian frequency.

However, the main drawback of STFT is a trade-off between time and frequency resolution depending on the length of smoothing window. In general, STFT does not have the capability to resolve overlapped multimodal reflections. In recent decades, the research on other representations for guided wave signal processing has been reported. For instance, Prosser *et al* [4] utilized the Pseudo Wigner-Ville Distribution for damage detection in multilayered structures and Pines used the Hilbert–Huang transform [5]. Continuous Wavelet and Chirplet Transforms were presented in the work by Kerber [6]. De Marchi *et al* [7] introduced a special operator to tile the time-frequency plane in a warped fashion that matches the group velocity curves of different materials. However, many of these works were mainly focused on obtaining the dispersion properties of the structure, which is not very practical for online monitoring applications that require minimal signal spreading.

2.2 Reassigned spectrogram with chirp transform kernel (RSCT)

The reassigned TFRs belong to another class of representations that has recently gained attention in GW analysis. The reassignment procedure substantially reduces the blurriness of the TFR and improves its mode identification capabilities. Even though the idea has been applied to different representations, the STFT-based reassigned spectrogram (RS) emerged as the best candidate for resolving multiple, closely spaced GW modes [8]. Reassigned spectrogram moves the STFT values to the local energy centers or centroids of the Wigner-Ville Distribution [9]. We can express the STFT in terms of the Gabor Transform:

$$x(t) = \iint \epsilon(\tau,\omega) \cdot \Psi(t,\tau,\omega) d\tau d\omega \tag{2}$$

The coefficients of the transform are defined as

$$\epsilon(\tau,\omega) = \int_{-\infty}^{\infty} x(t) \cdot \Psi^*(t,\tau,\omega) dt \tag{3}$$

The window function of STFT is expressed in terms of $\Psi(t,\tau,\omega)$:

$$\Psi(t,\tau,\omega) = h(\tau - t) e^{-j\omega(\tau - t)} \tag{4}$$

The coefficients of the Gabor Transform have amplitude and phase modulation

$$\epsilon(\tau,\omega) = \int_{-\infty}^{\infty} x(t) \cdot h(\tau - t) e^{j\omega(\tau - t)} dt = e^{j\omega\tau} \int_{-\infty}^{\infty} x(t) \cdot h(\tau - t) e^{-j\omega t} dt = A(\tau,\omega) e^{j\Phi(\tau,\omega)} \tag{5}$$

The original signal can be reconstructed as

$$x(t) = \iint A(\tau,\omega) \cdot h(\tau - t) \cdot e^{j[\Phi(\tau,\omega) - \omega\tau + \omega t]} d\tau d\omega \tag{6}$$

where $\Phi(\tau,\omega)$ – phase of the STFT, τ – time lag variable, and ω – radian frequency.

The reassignment method is based on the phase stationarity principle to identify the local energy centers. In the case of Lamb wave signals, equation (6) represents the oscillatory integral over a function that fluctuates rapidly under a slowly varying envelope. The significant contributions to (6) come from the vicinity of points where the phase is stationary, that is, where it goes through zero [10], which yields

$$\frac{\partial}{\partial\omega}[\Phi(\tau,\omega) - \omega\tau + \omega t] = 0 \quad \text{and} \quad \frac{\partial}{\partial\tau}[\Phi(\tau,\omega) - \omega\tau + \omega t] = 0 \tag{7}$$

The remapped time and frequency coordinates of the spectrogram can be computed as

$$\hat{t}(\tau,\omega) = \tau - \frac{\partial\Phi(\tau,\omega)}{\partial\omega} \text{ and } \hat{\omega}(\tau,\omega) = \frac{\partial\Phi(\tau,\omega)}{\partial\tau} \tag{8}$$

where $-\frac{\partial\Phi(\tau,\omega)}{\partial\omega}$ – local group delay; $\frac{\partial\Phi(\tau,\omega)}{\partial\tau}$ – instantaneous frequency.

In this work, the reassigned spectrogram was implemented using the cross-spectral method, proposed by Nelson *et al* [11] in order to reduce the computational complexity of the algorithm. In addition, the resolution of RS was further improved by substituting its original FFT-based kernel by a Chirp Z-transform (CZT). CZT is an algorithm frequently used to compute any set of equally spaced samples of the Discrete Fourier Transform (DFT) for an arbitrary contour on a Z-plane [12].

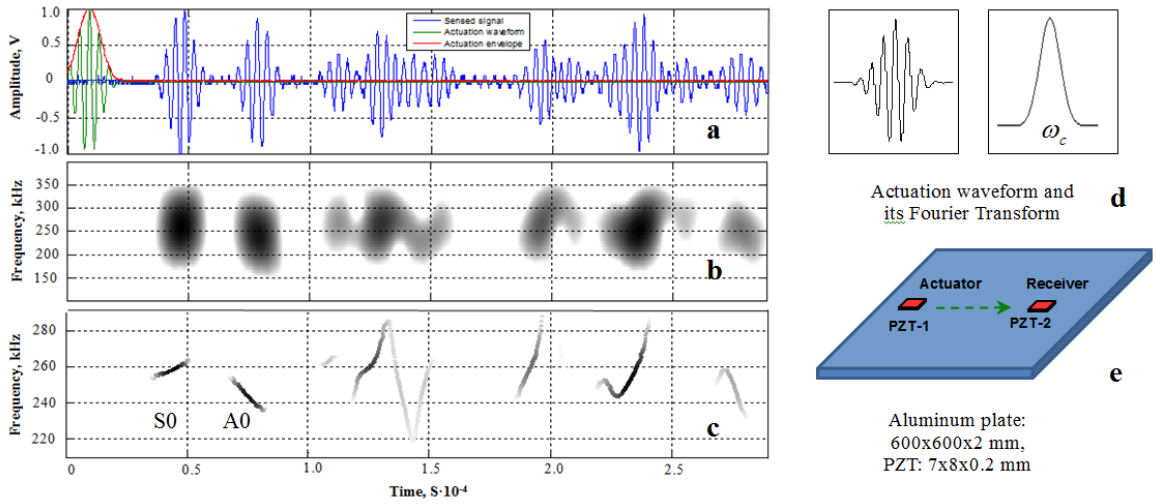

Fig. 2. a) Lamb wave signal (10240 samples); b) STFT (win-size=350); c) RSCT d) Experimental set-up

Or, equivalently, it provides zooming into a narrowband frequency region of the signal in order to interpolate the details. Let $x[n]$ denote a signal and $X(e^{j\omega})$ its Fourier transform. Consider evaluation of a circular segment on a *Z*-plane having *M* equally spaced points

$$\omega_k = \omega_0 + k\Delta\omega, \quad k = 0,1...M-1 \tag{9}$$

The DFT of the signal can be expressed in terms of the chirp $W = e^{j\Delta\omega}$:

$$X(e^{j\omega_k}) = \sum_{n=0}^{N-1} x[n]\cdot e^{-j\omega_k n} = \sum_{n=0}^{N-1} x[n]\cdot e^{-j\omega_0 n} W^{nk} \tag{10}$$

Using the identity $nk = \frac{1}{2}[n^2 + k^2 - (k-n)^2]$, we can derive the final expression for CZT:

$$X(e^{j\omega_k}) = \sum_{n=0}^{N-1} x[n]\cdot e^{-j\omega_0 n} W^{n^2/2} W^{k^2/2} W^{-(k-n)^2/2} = W^{k^2/2}\left(\sum_{n=0}^{N-1} g[n]\cdot W^{-(k-n)^2/2}\right) \tag{11}$$

The proposed time-frequency representation or Reassigned Spectrogram with Chirp Transform kernel (RSCT) was implemented to zoom into the narrowband range around the peak actuation frequency and run the reassignment procedure by Nelson. Fig.2b and Fig.2c demonstrate the original STFT and RSCT of Lamb wave signal obtained on 2-mm thick aluminum plate. This paper takes advantage of the improved resolution of RSCT to identify different Lamb wave modes. The narrowband actuation of guided waves (e.g. Morlet wavelet, Fig.2d) on any non-flat region of dispersion curves (Fig.1a) introduces a difference between the velocities of lower and higher frequency components of the generated wave packets. Consider the group delay of a single wave packet [14]:

$$\tau_g(\omega) = \frac{d\varphi(\omega)}{d\omega} = \frac{d(k(\omega)x_0)}{d\omega} = \frac{x_0}{d\omega/dk(\omega)} = \frac{x_0}{\upsilon_{gr}(\omega)} \tag{12}$$

where $\varphi(\omega)$ – phase of the actuation waveform, $k(\omega)$ – wavenumber, x_0 – propagation distance.

The group delay is in inverse relation with the group velocity, hence for a given narrowband actuation frequency range, the group delay slope of S0 mode is positive and that of A0 is negative. This correlation is clearly reflected in the RSCT of the signal (Fig.2c). Therefore, information about the mode can be extracted from the slopes of the RSCT time-frequency 'ridges'.

3. Matching pursuits for Lamb wave signal analysis

3.1. Matching Pursuits with conventional dictionaries

The MP algorithm decomposes the signal into a linear combination of functions (atoms) from an overcomplete frame *D,* called a dictionary [13]:

$$x = \sum_{n=0}^{N-1} \alpha_n \phi_{\gamma n}, \quad \phi_{\gamma n} \in D \tag{13}$$

where x – input signal, α_n – weight coefficients, $\phi_{\gamma n}$ – dictionary functions.

Given a dictionary with unit norm atoms, let R_n be the residual at n^{th} approximation of a signal x. MP projects the signal onto the elements of D in order to find the element that has the highest correlation with R_n. This iterative scheme consists of the following steps:

1. Specify initial conditions: $R_0 x = x$;
2. Find the atom with the highest inner product: $\phi_{\gamma n} = \arg\max \left\langle \left| R_{n-1}, \phi_{\gamma} \right| \right\rangle$ (14)
3. Subtract chosen atom from the signal and update the residual: $R_n = R_{n-1} - \left\langle R_{n-1}, \phi_{\gamma n} \right\rangle \cdot \phi_{\gamma n}$ (15)
4. Stop the algorithm when the residue energy is sufficiently small or the maximum number of iterations n_{max} is exceeded.

One of the key properties of MP that makes it useful for GW monitoring applications is its robustness to noise. This follows from the fact that the dictionary contains only predefined noise-free functions. In addition, MP tries to find the sparsest decomposition (e.g. linear combination requiring the least number of basis-functions). For a properly constructed basis, the solution would be sparser if more atoms are used. However, this increases the complexity of the problem and in general, it is non-polynomial hard. Therefore, the choice of dictionary plays an essential role in MP decomposition. In GW analysis, elements of D are chosen to have shapes similar to those of ultrasonic wave packets. Since Gabor and chirplet functions are very similar to oscillatory waveforms with short time support, the matching pursuit algorithm with these dictionaries has been explored by a number of researchers [14-16]. A unit energy chirplet can be expressed as

$$\phi_{(s,u,\omega,c)} = \frac{1}{\sqrt{s}} g\left(\frac{t-u}{s}\right) \cdot e^{\left[j(\omega(t-u)+\frac{c}{2}(t-u)^2+\varphi) \right]} \tag{16}$$

where: s – scaling factor, u – translation; c – chirp rate; $g(x)$ – modulation function; φ – initial phase.

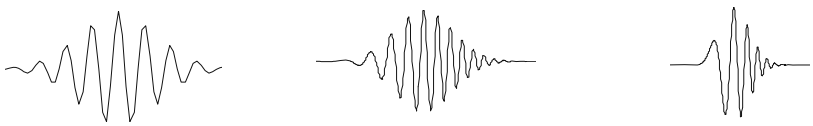

Fig. 3. Atoms of conventional MP dictionaries: Gabor and two chirplets with different scales

If c = 0, the atom degrades to a Gabor function (Fig.3). However, the implicit assumption in these works is that the signals are either non-dispersive or have a linear phase velocity. In general, the atoms of such dictionaries are ill-suited for analyzing dispersive wave packets at long propagation distances from the actuator, where the envelope of the wave packet is not necessarily Gaussian-shaped. Furthermore, numerically computed atoms are not tiled to the propagation distance explicitly. As a result, MP algorithm needs to compute a large number of inner products along all possible time samples in order to find the best projection. With such dictionaries, the decomposition tends to be slow (redundant dictionary that includes all possible shifts of atoms), inaccurate (coarse dictionary) or, finally, it may require interpolation after each iteration. From this perspective, dispersion based dictionary offers more precise analysis of the signal's mode content.

3.2. Matching Pursuit with dispersion-based dictionary

Dispersion based dictionary for MP decomposition of ultrasonic signals was first proposed by Hong *et al* [17]. In such a dictionary, atoms correspond to snapshots of wave packets at a distance x_n from the actuator. Each atom can be generated in the frequency domain and then transformed into the time domain:

$$\phi_{\gamma n} = iFT\{M(\omega)\cdot e^{-jk(\omega)x_n}\} \tag{17}$$

where $\phi_{\gamma n}$ – dictionary atom, $M(\omega)$ – FT of Morlet wavelet and $k(\omega)$ – wavenumber.

Equation 17 assigns different phase velocities to the Fourier components of the actuation waveform by considering the corresponding wavenumbers. As a result, the atoms realistically simulate the dispersion of Lamb waves (Fig.4).

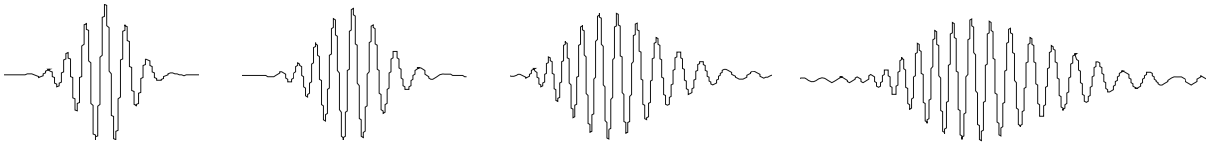

Fig.4. Generated atoms of A0 mode propagating in 2 mm thick aluminum plate at 0.25 m, 0.5 m, 1.0 m and 1.5 m from the actuator. Actuation waveform: 250 kHz, 5 cycle Hann windowed sinusoid.

However, in the case of surface-bonded piezoelectric wafer sensors the magnitude of each frequency component transferred to the structure depends not only on the shape of the Morlet wavelet, but also on the geometry and material properties of PZT [18]. Hence, the minor compensation for energy transfer conditions can be included into $M(\omega)$ to achieve more accurate decomposition.

4. Two-stage Mode Decomposition algorithm

Efficient implementation of Mode Decomposition algorithm is critical for online monitoring applications that require minimal time for signal processing. Since MP is iterative it becomes computationally intensive. However, the structure of dispersion-based dictionary can be exploited to substantially decrease its complexity. In fact, each element of such a dictionary has a short time support *L* compared to the length of the signal *N* in samples. Therefore, the speed-up can be achieved by local computation of inner products corresponding to the support *L* only. Furthermore, the set of computed correlations between two consecutive iterations of MP remains the same everywhere except at the support of the last atom chosen.

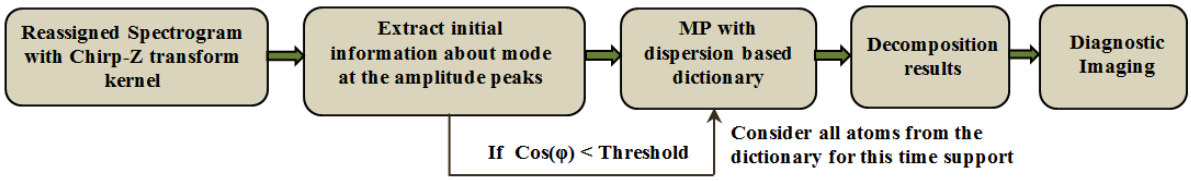

Fig.5. Flowchart of the two stage MD algorithm

As a result, previous comparisons between the inner products can also be stored in a tournament tree to make the search for the maximum in (14) faster. MP decomposition should be robust with respect to deviations between the assumed material properties of the structure and their real values. The difference in material's density, Young's modulus and Poison's ratio can affect the dispersion relations. Hence, the atoms of the dictionary are allowed to have the offset of *h* samples to the left and to the right from the simulated propagation distance to compensate for minor discrepancies in the group velocities. Therefore, each element of the dictionary in such decomposition generates a sequence of *2h+1* inner products that can be efficiently computed using FFT-based convolution. The computational cost of a single iteration of this MP algorithm requires approximately *LlogL*

computations.

The performance of MP can be further improved by utilizing the mode identification capabilities of RSCT. A schematic of such a two-step MD method is presented on Fig.5. The initial information about the mode of the wave packet is extracted from the slope of the group delay on the RSCT-image (Fig.2c), which is evaluated at the peaks of the signal's envelope. The knowledge of the mode provides the opportunity to exclude the atoms corresponding to other modes during the MP decomposition, thereby making it faster. Unfortunately, linear superposition of more than two wave packets arriving at the receiver with close TOFs, can distort the instantaneous frequency and, in this case, the slope of the group delay may not be a reliable measure of the mode. Therefore, MP starts with the RSCT-supplied modes first, but then checks the quality of projection by evaluating the angle φ between the atom-function and the corresponding support of the signal. If the latter is small enough, the RSCT-proposed projection is subtracted from the residual, otherwise, all possible atoms are considered.

5. Probability Diagnostic Imaging

Probability Diagnostic Imaging (PDI) allows the online monitoring system to visualize structural damage and assess it quantitatively [3]. The method may combine pulse-echo and pitch-catch configurations of sensors in an active network to acquire signal features associated with damage. In combination with MD, damage location could be easily identified by measuring the TOF of each decomposed Lamb wave mode reflected by the anomaly. This TOF includes the time required for the wave packet to travel from the actuator to the defect and the time to reach from defect to the receiver. Hence, the TOF corresponding to the reflection from damage can be computed using the equation

$$\frac{L_{Ai-D} + L_{D-Ri}}{\upsilon_{gr}} = TOF_i \tag{18}$$

where L_{Ai-D} – distance from the i_{th} actuator to defect; L_{D-Si} – distance from the defect to the the i_{th} sensor; υ_{gr} – group velocity of MD-identified Lamb wave mode evaluated at the peak actuation frequency.

It follows that damage must be located on the locus of an ellipse defined by L_{Ai-D} and L_{D-Si} for each actuator-receiver pair. PDI assigns the 2D Gaussian probability density function to each pixel on every ellipse of the array. As a result, the regions of the image where more of the ellipses overlap are illuminated intensively, indicating the most probable location of the damage (Fig.11b).

6. MD-based Diagnostic Imaging. Demonstration of the algorithm's capabilities

6.1 Demonstration of Mode Decomposition method

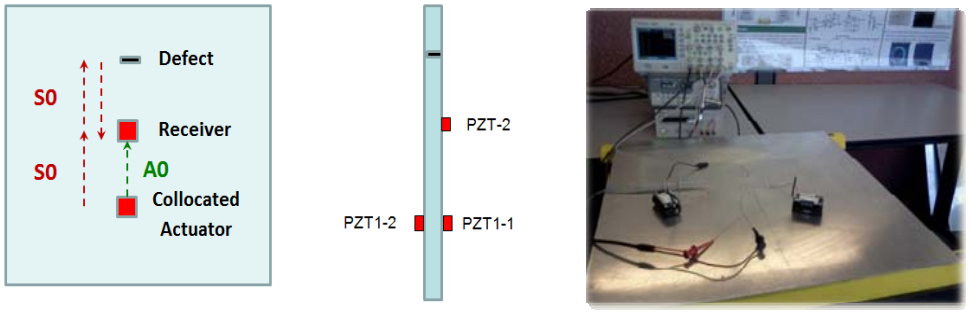

Fig.6. a) 600x600x2 mm aluminum plate; b) collocated actuator, side-view; c) experimental set-up.

Performance of the proposed MD method was tested on 2-mm thick 6061-aluminum alloy plate with a notch (Fig.6). Lamb waves were generated with a pair of collocated 7×8×0.2 mm transducers PZT1-1, PZT1-2 and were sensed by the receiver PZT-2. Morlet wavelet excitation (10V) at 250 kHz

center frequency was applied to PZT-1 using the arbitrary waveform generator 33220A (Agilent, Inc.) in order to activate S0 and A0 modes in the plate. Data were sampled from the output of the charge amplifier with the help of the digital oscilloscope DSO1004 (Agilent, Inc.).

For a given plate thickness, both S0 and A0 modes have high energy, therefore neither of them can be ignored in the analysis. In the set-up in Fig.7, S0 mode gets reflected from the defect before A0 reaches the receiver, hence their wave packets arrive with close TOFs. In order to test the MD, Lamb waves are first actuated with a single surface bonded PZT1-1 and then, with the collocated PZT pair. Out-of-phase activation of PZT-1 reduces the energy of S0 mode and forces the received signal to become nearly unimodal A0. This fact is later used to verify the decomposition results.

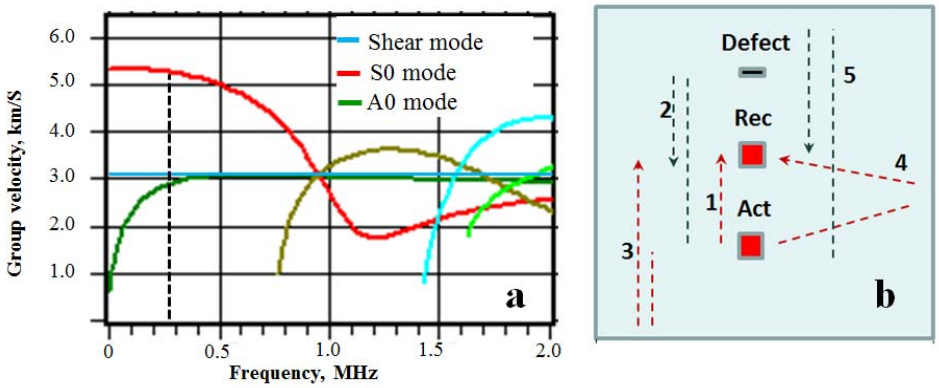

Fig.7. a) Dispersion curves and actuation frequency; b) wave paths

Wave path	Length, cm	ToF-S0, μs	ToF-A0, μs
1	14.5	28.4	52.0
2-def	36.5	71.5	130.5
3	53.1	104.1	--
4	62.0	121.4	--
5	66.5	130.2	--

Table 1. Analytically predicted TOFs of different modes

Given the group velocities V_{S0} = 5150 m/s, V_{A0} = 2788 m/s, V_{shear} = 3070 m/s (Fig.7a), it is possible to predict the TOF of wave packets analytically for this simple geometry. The shortest possible wave paths are shown in Fig.7b and the corresponding TOFs are presented in Table 1.

Two signals (10240 samples each) corresponding to a single and collocated PZT actuation (Fig.8), were subjected to the MD algorithm, described in the previous sections. Dictionary used for MP included 482 atoms: the Gabor atom for shear waves, 241–A0 and 261–S0 atoms to simulate possible propagation of wave packets for a maximum distance corresponding to the time-length of the signal. Each atom was allowed to have a shift of 70 samples from its simulated position. The threshold for the cosine of the angle between the TFR-proposed wave-packets and the local support of the signal was set to 0.9. MP converged after 7 iterations to the residual energy (5% of initial level).

Separated modal components of the signal obtained with a single PZT actuation are presented in Fig.9. Comparing the results with analytical calculations (Table 2), we see that MD has correctly extracted the TOF of S0 and A0 defect reflections and, at the same time, identified the incident S0, A0 and shear mode wave packets.

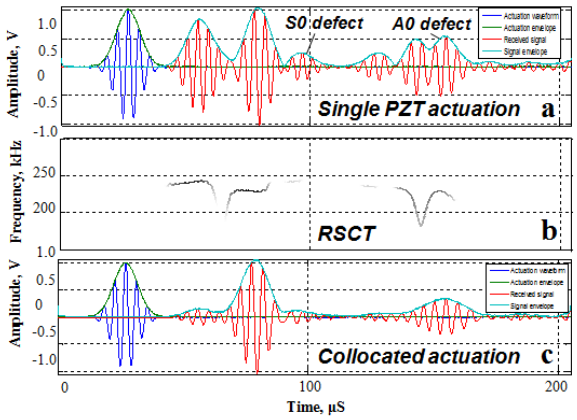

Fig.8. Experimental data: a) Lamb wave signal recorded on the receiver after single PZT actuation; b) RSCT of the signal; c) Signal recorded on the receiver after collocated actuation.

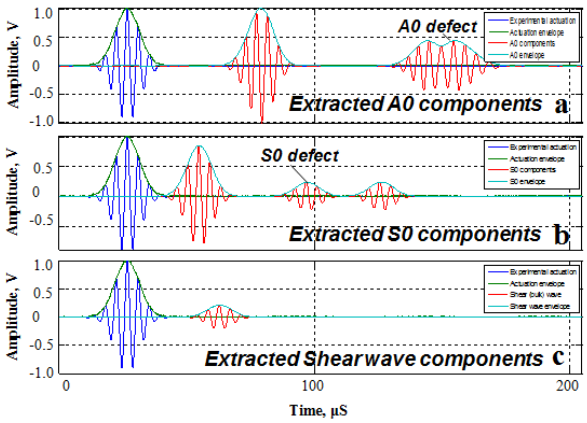

Fig.9. Decomposition results: a) extracted A0 atoms; b) extracted S0 components; c) extracted shear mode components.

Number of wave path	1	2-defect	3	4	5
SO Analytical / MD-based ToF, μs	28.4/30.2	71.5/69.5	104.1/102.1	121.4/--	130.2/--
SO Experimental / MD-based Distance, cm	14.5/15.5	36.5/37.2	53.1/52.6	62.0/--	66.5/--
AO Analytical / MD-based ToF, μs	52.0/50.5	130.9/132	--	--	--
AO Experimental / MD-based Distance, cm	14.5/15.2	36.5/35.9	--	--	--

Table 2. Comparison of analytically predicted and MD-extracted TOFs and propagation distances.

The signal reconstructed as a superposition of A0-selected atoms, correlates well with the experimental waveform obtained with the collocated PZT set-up (Fig.8c and Fig.9a). Hence, the MD algorithm can be utilized to provide diagnostic imaging in the case when more than one high-energy mode is present in the structure. In particular, such an approach can be implemented without a baseline if the defect is large enough to be considered a strong reflector. Otherwise, the algorithm should be applied to the differenced signal.

6.2. Diagnostic Imaging results

The MD-based PDI was tested on the similar 60×60 cm and 2-mm thick aluminum plate, but with a different positioning of sensors shown in Fig.11a. The method used Lamb wave data recorded for each pair of sensors in pitch-catch configuration.

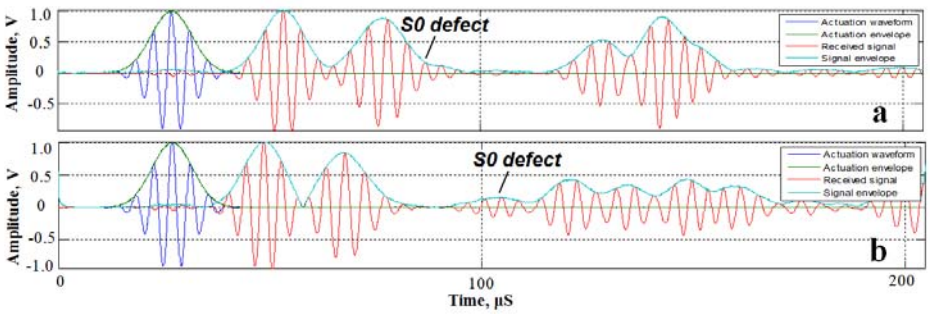

Fig.10. a) Signal from PZT 2-3 sensor pair; b) signal from PZT 1-2 sensor pair.

Reflections of S0 mode were chosen to identify the defect location. Typical sampled signals are presented in Fig.10. It should be noted that S0 reflection from damage had minimal overlap with other

wave packets in the signal obtained from sensor pair PZT1-PZT2. However, for a sensor pair PZT1-PZT3, it merged with A0 incident wave packet. In this case, the capabilities of MD algorithm were fully exploited to extract information about the overlapped modes and their TOFs.

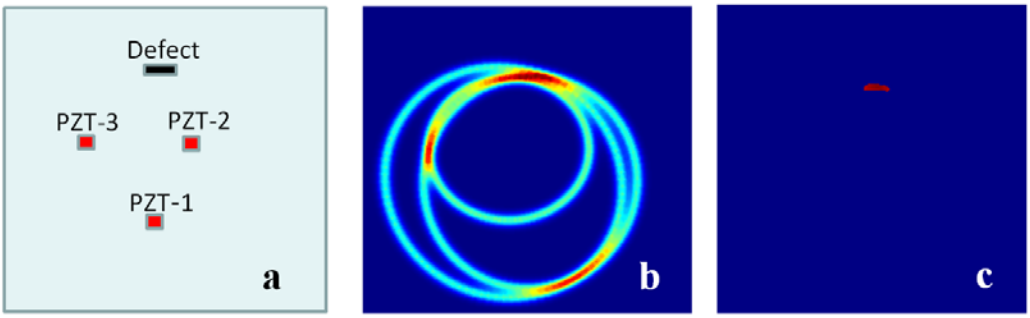

Fig.11. a) Experimental set-up; b) PDI-generated ellipses; c) identified defect location.

The S0 mode components resulting from MD were utilized as an input for a standard PDI algorithm. Ellipses computed for each sensor pair were merged and thresholded to obtain the most probable damage location. The coordinates identified for the damage location was within a deviation of less than 1 cm from its true geometric coordinates of the machined defect (Fig.11c).

7. Conclusion

This paper presented a new approach for processing of multimodal Lamb wave signals. Two-stage Mode Decomposition algorithm, employing the Reassigned Spectrogram with Chirp Transform kernel and Matching Pursuit with dispersion-based dictionary, was proposed to identify and separate high energy S0 and A0 wave packets propagating in aluminum plates. It was demonstrated that MD-extracted information about the mode, amplitude, Time-of-Flight (ToF) and distance travelled by each reflection could be efficiently used to identify the location of the defect with the help of Probability Diagnostic Imaging. Future work will focus on the application of proposed algorithm to industrial pipes, composite materials and structures with more complicated geometry.

References

[1] T. Stepinski, Structural Health Monitoring of Piping in Nuclear Power Plants, Swedish Radiation Safety Authority, Report number 2011:17, 2011.
[2] J.L. Rose, Ultrasonic waves in solid media, Cambridge University Press, 2004.
[3] C. Zhou, Z. Su and L. Chen, Probability-based diagnostic imaging using hybrid features extracted from ultrasonic Lamb wave signals, Smart Materials and Structures 20 (2011).
[4] W. Prosser, N. Seale and B. Smith, Time-frequency analysis of the dispersion of Lamb modes, Journal of Acoustical Society of America 105 (1999), 2669–2676.
[5] D. Pines and L. Salvino, Structural health monitoring using empirical mode decomposition and the Hilbert phase, Journal of Sound and Vibration 294 (2006), 97–124.
[6] F. Kerber, H. Sprenger, M. Niethammer, K. Luangvilai and L. Jacobs**,** Attenuation Analysis of Lamb Waves Using the Chirplet Transform, EURASIP Journal on Advances in Signal Processing, 2010.
[7] L. De Marchi, A. Marzani, S. Caporale, N.Speciale, Ultrasonic guided-waves characterization with warped frequency transforms, IEEE Trans. Ultrason. Ferroelectr. Freq. Control 56(10) (2009), 2232–2240.
[8] M. Niethammer, L. Jacobs, Time-frequency representation of Lamb waves using the reassigned spectrogram, Acoustics Research Letters, 2000.
[9] P. Flandrin, F. Auger and E. Chassande-Mottin, Applications in Time-Frequency Signal Processing, CRC Press, 2002, 179–201.
[10] A. Rihaczek, Signal energy distribution in time and frequency, IEEE Transactions on Information Theory, 14 (1968), 369–384.

[11] D. Nelson, Cross-spectral methods for processing speech, Journal of Acoustical Society of America 110(5) (2001), 2575-2592.
[12] A. Oppenheim and R. Schafer, Discrete-time signal processing, Prentice Hall, 1999, 656–661.
[13] S.G. Mallat, and Z. Zhang, Matching pursuits with Time-Frequency dictionaries, IEEE Transactions on Signal Processing, 41 (1993), 3397–3415.
[14] B. Xu, V. Giurgiutiu and L. Yu, Lamb Waves Decomposition and Mode Identification Using Matching Pursuit Method, Sensors and Smart Structures, Technologies for Civil, Mechanical, and Aerospace Systems 7292, (2009).
[15] A. Raghavan and C. Cesnik, Guided-wave signal processing using chirplet matching pursuits and mode correlation for structural health monitoring, Smart Materials and Structures 16 (2007), 355–366.
[16] Y. Li and J. Michacls, Numerical Implementation of matching pursuit for the analysis of complex ultrasonic signals, IEEE Trans. Ultrason. Ferroelectr. Freq. Control, 55 (2008), 173-182.
[17] J. C. Hong, K. H. Sun and Y. Y. Kim, Waveguide damage detection by the matching pursuit approach employing the dispersion-based chirp functions, IEEE Trans. Ultrason. Ferroelectr. Freq. Control, 53 (2006), 592–605.
[18] A. Raghavan and C. Cesnik, Finite-dimensional piezoelectric transducer modeling for guided wave based structural health monitoring, Smart Materials and Structures. 14 (2005), 1448–1461.